Original Article

Crosstalk between aryl hydrocarbon receptor (AhR) and BCL-2 pathways suggests the use of AhR antagonist to maintain normal differentiation state of mammary epithelial cells during BCL-2 inhibition therapy

Abdullah Al-Dhfyan [a,b], Ayodele Alaiya [a], Falah Al-Mohanna [c], Mohamed W Attwa [d], Abdullah F AlAsmari [a], Saleh A Bakheet [a], Hesham M. Korashy [e,*]

[a] Department of Pharmacology and Toxicology, College of Pharmacy, King Saud University, Riyadh 11451, Saudi Arabia
[b] Stem Cell & Tissue Re-Engineering Program, King Faisal Specialist Hospital and Research Center, Riyadh 11211, Saudi Arabia
[c] Department of Comparative Medicine, King Faisal Specialist Hospital and Research Center, Riyadh 11211, Saudi Arabia
[d] Department of Pharmaceutical Chemistry, College of Pharmacy, King Saud University, Riyadh 11451, Saudi Arabia
[e] Department of Pharmaceutical Sciences, College of Pharmacy, QU Health, Qatar University, Doha 2713, Qatar

HIGHLIGHTS

- Activation of the AhR/CYP1A1 increased EpCAM^{High}/CD49f^{Low} CD61$^+$ luminal progenitor-like cells *in vivo* mice model.
- Activation of the AhR/CYP1A1 pathway increased BCL-2 expression and activity *in vitro* and *in vivo*.
- Activation of BCL-2 increased the expression of the pluripotency factors *in vitro* and *in vivo*, while its inhibition by venetoclax prevented CSC expansion and chemoresistance.
- Venetoclx treatment alone increased EpCAM^{High}/CD49f^{Low} CD61$^+$ luminal progenitor-like cells causing inhibition of epithelial lineage markers and disruption of mammary gland branching.
- Combined treatment of VCX with AhR antagonist in mice corrected the abnormal differentiation in mammary epithelial cells and protected mammary gland branching and cell identity.

GRAPHICAL ABSTRACT
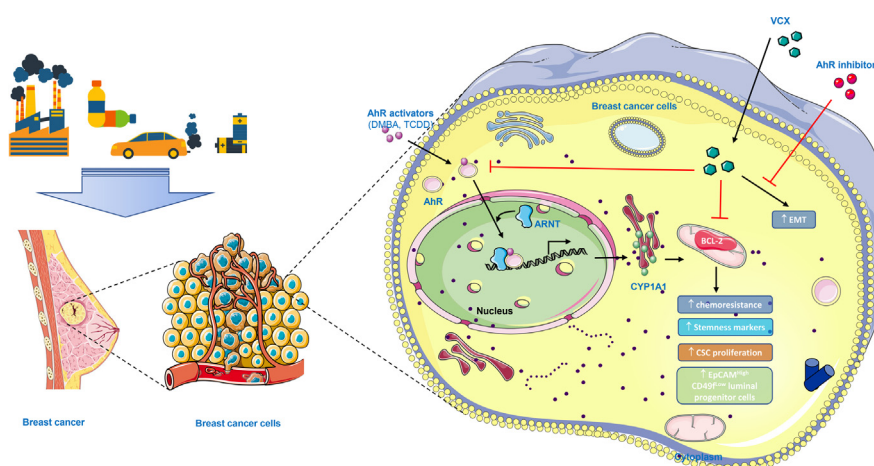
ARTICLE INFO

ABSTRACT

Introduction: Activating the aryl hydrocarbon receptor upon exposure to environmental pollutants promotes development of breast cancer stem cell (CSCs). BCL-2 family proteins protect cancer cells from the apoptotic effects of chemotherapeutic drugs. However, the crosstalk between AhR and the BCL-2

A. Al-Dhfyan, A. Alaiya, F. Al-Mohanna et al.

family in CSC development remains uninvestigated.

Objectives: This study explored the interaction mechanisms between AhR and BCL-2 in CSC development and chemoresistance.

Methods: A quantitative proteomic analysis study was performed as a tool for comparative expression analysis of breast cancer cells treated by AhR agonist. The basal and inducible levels of BCL-2, AhR, and CYP1A1 *in vitro* breast cancer and epithelial cell lines and *in vivo* mice animal models were determined by RT-PCR, Western blot analysis, immunofluorescence, flow cytometry, silencing of the target, and immunohistochemistry. In addition, an *in silico* toxicity study was conducted using DEREK software.

Results: Activation of the AhR/CYP1A1 pathway in mice increased EpCAM^{High}/CD49f^{Low} CD61$^+$ luminal progenitor-like cells in early tumor formation but not in advanced tumors. In parallel, a chemoproteomic study on breast cancer MCF-7 cells revealed that the BCL-2 protein expression was the most upregulated upon AhR activation. The crosstalk between the AhR and BCL-2 pathways *in vitro* and *in vivo* modulated the CSCs features and chemoresistance. Interestingly, inhibition of BCL-2 in mice by venetoclax (VCX) increased EpCAM^{High}/CD49f^{Low} CD61$^+$ luminal progenitor-like cells, causing inhibition of epithelial lineage markers, disruption of mammary gland branching and induced the epithelial-mesenchymal transition in mammary epithelial cells (MECs). The combined treatment of VCX and AhR antagonists in mice corrected the abnormal differentiation in MECs and protected mammary gland branching and cell identity.

Conclusions: This is the first study to report crosstalk between AhR and BCL-2 in breast CSCs and provides the rationale for using a combined treatment of BCL-2 inhibitor and AhR antagonist for more effective cancer prevention and treatment.

Introduction

A hallmark of cancer is chemoresistance and cancer relapse, a feature that is mediated by the presence of cancer stem cells (CSCs). CSCs are a small subgroup of cells in the tumor mass with unlimited proliferative and self-renewal capacity [1]. Chemotherapy treatment often results in increased percentages of CSCs in humans and animals [2,3], providing insights into the mechanisms of cancer recurrence following chemotherapy treatment observed in many cases. Notably, a low dilution number of only 200 CSCs can form breast tumors in immunocompromised mice. In contrast, transplantation of 20,000 differentiated cells showing the same marker expression fails to form tumors, demonstrating the tumorigenic potential of CSCs [4]. Therefore, CSCs have been a significant focus in cancer research, and many studies have been performed to develop efficient CSC-targeted therapeutic strategies that can eradicate tumors and ultimately improve patient clinical outcomes.

CSCs are regulated by many self-renewal pathways, including Wnt and Notch [5]. Several recent *in vitro* and *in vivo* studies demonstrated that the aryl hydrocarbon receptor (AhR) regulates CSC proliferation, self-renewal, stemness markers, and resistance to chemotherapy regimens through PTE/AKT and WNT/β-catenin mechanisms [6,7]. AhR is a cytoplasmic transcription factor that plays a significant role in regulating cell fate and multiplication [8,9]. The activation of AhR upon binding to its ligands, such as TCDD and 7,12-dimethybenz[*a*]anthracene (DMBA), induces the transcriptional expression of its downstream target genes, CYP1A1 and CYP1B1 [10,11]. As a result, CYP1A1 and CYP1B1 bioactivate environmental compounds to their ultimate carcinogenic epoxide derivatives, causing DNA adducts that trigger mutations [12]. The failure of DMBA to induce tumors in CYP1-knockout mice supports the tumorigenic role of AhR/CYP1A genes [13].

The treatment-resistance properties of CSCs can be attributed to many factors, including the non-proliferative nature of stem cells, microenvironment, overexpression of anti-apoptotic genes, and activation of DNA repair pathways [14]. Among these factors, the anti-apoptotic protein BCL-2 is known to be overexpressed in about 75 % of breast cancer cases [15], suggesting its role in chemoresistance and cancer recurrence. Mechanistically, the anti-apoptotic BCL-2 family proteins regulate apoptosis in a mitochondrion-dependent manner by inhibiting pro-apoptotic proteins, such as Bax and Bad [16]. Thus, targeting the BCL-2 protein family is being investigated in preclinical studies as a novel therapeutic strategy against cancer. In this context, the US FDA has recently approved venetoclax (VCX) as an oral BCL-2 inhibitor for treating patients with chronic and small lymphocytic lymphoma [17].

Linking the controlling effect of AhR/CYP1A1 on CSC proliferation with the overexpression of BCL-2 in breast cancer has encouraged us to investigate the crosstalk between AhR/CYP1A1 and BCL-2 family in breast cancer and CSCs. For this purpose, *in vitro* human and *in vivo* mice breast cancer models were used to a) explore the potential molecular mechanisms through which AhR/CYP1A1 signaling regulates the expression and function of BCL-2, b) evaluate the role of BCL-2 inhibitor VCX in the AhR/CYP1A1-BCL-2 pathway mediated chemoresistance and CSC expansion, and c) explore the combined effect of AhR inhibitor and BCL-2 inhibitor on the differentiation state of mammary epithelial cells and breast cancer and CSC development.

Materials and methods

Materials

TRIzol reagent and apoptosis/necrosis kits were purchased from Invitrogen Co. (Grand Island, NY). AhR pharmacological activators and inhibitors were purchased from Toronto Laboratories Research (Toronto, Canada). RNA isolation and RT-PCR kits were obtained from Applied Biosystems® (Foster City, CA). Acrylamide/bisacrylamide 30% (29:1) and Western blot assay reagents were purchased from Bio-Rad Laboratories (Hercules, CA). Antibodies against target proteins and the manufacturing companies are listed in Suppl. Tab. 1. Interference RNA, transfection reagents and kits were ordered from Santa Cruz Biotechnology, Inc. (Santa Cruz, CA).

Breast cancer cell culture model

Human breast cancer cell lines MCF-7 (estrogen positive), MDA-MB-468 and Hs578T (triple-negative, TNBC), and human mammary epithelial (HMLE) cells were obtained from ATCC (Rockville,

A. Al-Dhfyan, A. Alaiya, F. Al-Mohanna et al.

MD). The MCF-7, MDA-MB-468, and Hs578T cells were maintained in DMEM with phenol red, supplemented with fetal bovine serum (10%), L-glutamine (200 μM), and 1X antibiotic–antimycotic. HMLE cells were cultured in DMEM-F12 supplemented with fetal bovine serum (10%), 1X antibiotic, hydrocortisone (0.5 μg/ml), insulin (10 μg/ml), and recombinant human EGF (20 ng/ml) at 37 °C under a 5% CO_2 humidified environment. In all experiments, all compounds were prepared fresh in dimethyl sulfoxide (<0.1% v/v).

Protein in-solution digestion and identification by high-resolution liquid chromatography/mass spectrometry (LC/MS)

Protein identification and qualitative expression were performed using one-dimensional Nano Acquity liquid chromatography coupled with tandem mass spectrometry on Synapt G2 HDMS (Synapt G2; Waters, Manchester, UK), using 2 ng/μL leucine enkephalin (556.277 Da). The mass (m/z) calibration was maintained using Mass Lynx IntelliStart. All analyses were performed using Triazaic Nanosource ionization (Waters™, USA) in the positive ion mobility mode with nanoelectrospray ionization [18].

Mammosphere formation (self-renewal) assay

Approximately 1000 MCF-7 and Hs578T cells/100 μL cultured in mammary epithelium basal medium with supplements were plated into ultralow attachment plates as described previously [19,20]. After seven days, both non-adherent (CSCs mammosphere) and adherent cells were treated for 72 h with the indicated compounds. After that, the number and size of the spheroid cells were measured by Evos® transmitted light microscope.

RNA isolation and real-time PCR (RT-PCR)

Total RNA was isolated using TRIzol reagent (Invitrogen®), and the RNA quality was maintained at a 260/280-absorbance ratio of ∼ 2.0 OD as described previously. The cDNA was synthesized, and the mRNA expression of target genes was quantified using human primers for BCL-2 (F: ACGAGTGGGATGGGGGGAGATGTG and R: GCGGTAGCGGCGGGAGAAGTC), CYP1A1 (F: CTATCTGGGCTGTGG GCAA and R: CTGGCTCAAGCACAACTTGG), and β-ACTIN (F: TATTGGCAACGAGCGGTTCC and R: GGCATA-GAGGTCTTTACGGATGTC) [6] using QuantStudio® 6 Flex Real-Time PCR System (Life Technologies Co., Grand Island, NY) [21]. The mRNA expression levels of target genes in all samples were calculated using the ΔΔ CT method [22].

Immunofluorescence analysis (IF)

MCF-7, MD-MB-468, and Hs578T cells (20000 cells/cm²) were plated on glass slides for seven days and then fixed in 4% formaldehyde to perform an IF assay as described previously [23]. The fixed cells were stained with antibodies against target proteins, followed by conjugated secondary antibodies and 1 μg/mL of DAPI. The fluorescence intensity and intracellular localization were examined by an Olympus immunofluorescence microscope.

Identification and evaluation of CSCs by side population (SP)

The SP analysis was conducted as described earlier [6]. Briefly, treatment MCF-7, MDA-MB-468, and Hs578T cells with tested compounds for 72 h were suspended in a DMEM cell culture medium followed by incubation with Dye Cycle Violet (DCV, 10 μM) and Propidium iodide (PI). The percentage of cells that appeared in the flow cytometry plot (SP) as distinct dim 'tail' was identified and measured using FACSAria® flow cytometer cell sorter, BD Biosciences (San Jose, CA).

Western blotting

Total protein lysates isolated from MCF-7 and HMLE cells of approximately 30 μg were separated on 10% SDS-PAGE and then transferred to a nitrocellulose membrane as described before [24]. Protein membranes were incubated with primary antibodies against target proteins, and the protein bands were detected using horseradish peroxidase (HRP) chemiluminescence substrates and then visualized by C-DiGit® Blot Scanner, LI-COR Biosciences (Lincoln, NE) [6].

RNA interference and lentiviral transfection

Short hairpin RNA (shRNA) and Lentiviral transfection was conducted using the method of Al-Dhfyan et al. [6]. Approximately 5×10^4 MCF-7 cells were transfected with lentivirus AhR and CYP1A1 shRNA or their control shRNA. Cells with stable transfection, which were selected using puromycin (2 μg/ml), were trypsinized and then cultured in 6-well cell culture plates, followed by treatment with the indicated compounds for 72 h.

Animal models and experimental design

Virgin female BALB/C and Swiss albino mice (20–25 g) were provided by the Animal Care Center, College of Pharmacy, King Saud University (KSU). Nude mice (Jackson Laboratories, Bar Harbor, Maine, USA) were obtained from the King Faisal Specialist Hospital and Research Centre (KFSHRC). The mice were housed in filter-top cages in a specific pathogen-free facility (SPF) in a room environment maintained at 22 °C with a 12-h light–12-h dark cycle. The mice were randomly divided into two groups of six mice each. The control group received sesame oil (IP), and the treated groups received either DMBA (30 mg/kg) or VCX (30 mg/kg). For the combination treatment, mice received a single dose of VCX followed by twice doses of either metformin (MET, 40 mg/kg) or α-naphthoflavone (α-NF, 60 mg/kg, IP). After the indicated period, all animals were anesthetized and decapitated, and then the mammary fat pads were immediately excised and stored at −80 °C for subsequent experiments.

Xenograft experiment

HMLE cells cultured in DMEM/F12 medium were treated with VCX 5 μM for 3 days for 3 cycles, a concentration known to induce minimal toxicity to the cells. After that, approximately 1x10⁶ HMLE cells from both VCX-treated and control sets were mixed (1:1) with Matrigel and then injected subcutaneously into both sides of 5-week-old female nude mice, The Jackson Laboratory (Bar Harbor, ME). The tumor's length (L) and width (W) were measured every week with a caliper, and the tumor volume (V) was calculated using the equation V = 1/2 ($W^2 \times L$).

Ethics statement

All the animal experiments were conducted by the National Institutes of Health Guide for the Care and Use of Laboratory Animals (NIH Publications No. 8023, revised 1978). All experimentations involving mice were conducted in accordance with a standard protocol approved by KSU and KFSHRC Committees on the Care and Use of Laboratory Animals (Approval number KSU-SE-19–09).

Histopathology and immunohistochemistry (IHC)

Snap-frozen fresh mammary glands were sectioned into 8 μm, using a cryotome, Thermo Shandon Ltd. (Pittsburgh, PA), and

adhered to Superfrost slides, Thermo Fisher Scientific (Pittsburgh, PA). After overnight air drying, the sections were fixed in 4 °C cold acetone for 10 to 20 min, followed by a few min incubations in phosphate buffer saline (PBS, pH 7.4). The sections were incubated for 15 min with a blocking solution containing endogenous peroxidase, 0.3% hydrogen peroxide in PBS, and 0.1% sodium azide. After two washes in PBS, sections were blocked with 10% goat serum (Dako Corp.) for 60 min, followed by the addition of a primary antibody (1:100 dilution) overnight at 4 °C in a humidified chamber. After washing three times in PBS, the sections were stained for 30 min at room temperature with a Labeled Polymer (EnVision +) HRP detection kit [6]. After three times washing with PBS, the sections turned red, using the chromogen 3-amino-9-ethyl carbazole (Sigma), and were then counterstained for 1 min with Harris hematoxylin, Acros Organics (Morris Plains, NJ). All sections were examined under Zeiss A xiovert 40 CFL microscope, Carl Zeiss LLC (Thornwood, NY), and photographed by the same histopathologist.

Preparation of MECs for flow cytometry

Internal mammary glands were collected from 6-week-old female mice and then mechanically dissociated with a scalpel and razor blades. Immediately after isolation, the tissues were incubated for one h in a culture medium containing the digestive enzymes collagenase (600 U/mL) and hyaluronidase (200U/mL) at 37 °C and 5% CO_2 [25]. The resulting suspension from the digestion process was treated with 0.25% trypsin-ethylenediaminetetraa cetic acid for 2 min and then quenched with an equal volume of complete medium containing dispase (5 mg/mL) and DNase (0.1 mg/mL) for 3 min. The single-cell solution was filtered through a 40-μm mesh, and the dissociated cells were then frozen at − 80 °C for further analysis on a FACS LSRII, BD Biosciences (San Jose, CA).

In silico prediction of VCX toxicity/carcinogenicity using Derek and Sarah Nexus and XenoSite reactivity model

The chemical structure of VCX was imported into Sarah and Derek's software, which was standardized and then fragmented. Sarah's software further refines the similarity of the VCX structure to a training set of compounds. The overall prediction is exhibited as a conclusion about the Ames mutagenicity of VCX and a confidence rating in the prediction. The detection of the vulnerable sites reactive intermediate molecules to DNA and proteins with common traps for electrophiles, i.e., cyanide and glutathione, were predicted using the XenoSite reactivity module *in silico* experiments using XenoSite Reactivity Prediction Web Server (https://swami.wustl.edu/xenosite) [26].

Pharmacovigilance assessment of breast cancer incidence by VCX

The assessment of breast cancer incident cases as a serious adverse effect of VCX use was performed using the FDA FAERS pharmacovigilance database [27]. All claims of breast cancer cases reported by healthcare professionals, consumers, and pharmaceutical manufacturers during the period from 2017 to 2022 were collected, including complete information on patient demographics, drug regimens, reported country, and patient outcomes.

Statistical analysis

Significant differences between study groups as compared to control ($p < 0.05$) were determined by either student's *t*-test or ANOVA followed by Student–Newman–Keul's test using SigmaStat®, Systat Software Inc., (San Jose, CA).

Results

Induction of luminal dedifferentiation and expansion of EpCAM^High^/CD49F^Low^ CD61^+^ luminal progenitor-like cells in DMBA-induced breast tumor in mice

Initially, we sought to study the effect of AhR activation on MECs differentiation and explore which cell populations are targeted for chemical toxicity and tumor initiation. Therefore, we performed mammary breast cell profiling to trace the cell origin of DMBA-induced breast tumors to link it to AhR/CYP1A1's role in cancer initiation. For this purpose, female mice were treated with either vehicle (control) or DMBA 30 mg/kg (IP) once a week for two cycles. After one month, half of the mice were labeled as the DMBA-treated group, whereas the rest were kept until tumor formation by the same treatment regimen and labeled the tumor group. Thereafter, flow cytometric markers for mouse breast cell sub-populations of normal (untreated), DMBA-treated (DMBA), and DMBA-induced breast cancer (Tumor) were performed. Interestingly, the profiling assay shows strong induction of luminal progenitor cells and luminal cells as evidenced by an increased percentage of EpCAM^High^/CD49F^Low^ CD61^+^ luminal progenitor-like cells by 37% and 41%, respectively (Fig. 1a). This increase was detected in early tumor formation but not in the advanced tumor, suggesting initiation function. Notably, luminal progenitor cells represent a rare sub-population and constitute less than 2% of normal mammary cells. Basal-like sub-population is not significantly affected by DMBA treatment compared with luminal-like progenitor cells. Furthermore, a decrease in basal population cells was detected in DMBA-induced tumors compared with normal mammary cells. These results demonstrate that DMBA-induced breast tumors are of luminal origin and that luminal progenitor cells play a crucial role in this animal model of chemically induced breast carcinogenesis tumor initiation.

Proteomic analysis of MCF-7 cells treated with AhR/CYP1A1 pathway inducer

The effect of chemical activation of AhR by DMBA on the differentiation of MECs and induction of targeted toxicity toward luminal-like cells prompted us to study the effect of AhR activation on the whole breast cancer cell proteome using quantitative label-free nano MS-based method aiming at identifying a novel druggable target for both prevention and treatment intervention purposes. A proteomic study was performed as a comparative expression analysis of the cells treated by AhR/CYP1A1 agonist TCDD. A standard statistical analysis method, Principal Component Analysis (PCA), was used to correct multiple comparisons between sample mock and treated cells. The global protein expression profiles in human breast cancer MCF-7 cells upon activation of the AhR showed that approximately 1553 unique protein species were identified across all sample groups. Three hundred nine of these proteins were statistically significant (ANOVA, $p < 0.005$) with at least > 2-fold differences between the two sample groups. Among which 142 proteins were characterized in ingenuity pathway analysis (IPA) and were represented in other networks. Of particular importance to this study is the network involving cancer, cell cycle, cell death and survival, cellular development, cell growth and proliferation as presented in Fig. 1b, where red indicates an upregulated protein (BCL-2), and pink is indicative of downregulation. Solid lines indicate a direct connection, whereas broken lines indicate indirect interaction between molecules. Other molecules identified in this study are in grey. The massive upregulation of BCL-2 protein in response to TCDD treatment raised the question of the importance and role of BCL-2 protein in breast carcinogenesis
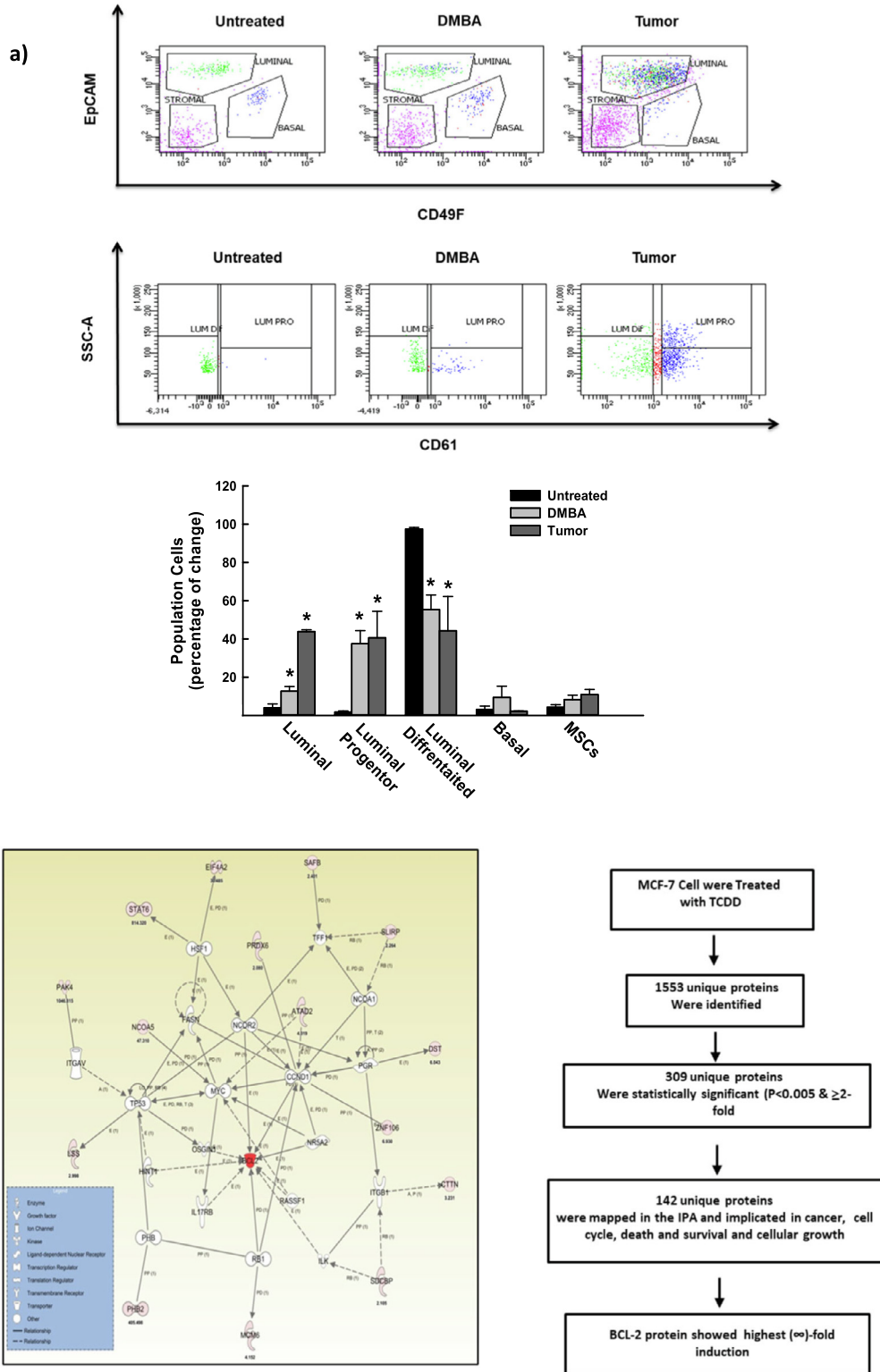
Fig. 1. Flow cytometric analysis of MECs and Proteomic analysis of MCF-7 cells treated with AhR/CYP1A1 inducer. a) Flow cytometric analysis was performed no MECs from mice treated with DMBA 30 mg/kg (DMBA) and DMBA-induced tumor (Tumor). The cell population of origin of DMBA-induced breast tumor involved in cancer initiation we performed by conducting mammary breast cell profiling using EpCAM, CD61, and CD49F. The values are presented as the mean of fold change ± SEM (n = 6) in triplicate. *; p < 0.05 compared to corresponding control (ANOVA followed by Student–Newman–Keul's test post hoc). **b)** Proteomic study was conducted on MCF-7 cells treated with TCDD (10 nM). Workflow and illustration of some of 142 of 309 identified proteins revealed in pathway analysis of signaling networks generated from the Ingenuity Pathway Analysis database (IPA). The Network analysis, connection and the expression profile of some of the identified proteins were generated using IPA V8.7.

A. Al-Dhfyan, A. Alaiya, F. Al-Mohanna et al.

and its crosstalk with the AhR/CYP1A1 pathway. Therefore, all subsequent studies and experiments aim to address this question.

Effect of AhR/CYP1A1 pathway activation on the expression of BCL-2 in vitro and in vivo models

To validate the upregulation of BCL-2 protein by TCDD, as evidenced by the proteomic analysis, we tested whether activation of the AhR/CYP1A1 pathway would increase the expression of BCL-2 *in vitro* human breast cancer cells and *in vivo* mice models. Fig. 2a shows that treating human mammary epithelial HMLE and human breast cancer MCF-7 cells for 48 h with two AhR inducers significantly increased BCL-2 protein level, associated with a proportional increase in the expression of AhR and CYP1A1 proteins. This effect was further evidenced by the IF study, in which treatment of breast cancer MCF-7 cells with either TCDD or DMBA significantly increased the cellular content and localization of BCL-2 and its phosphorylated protein in a manner similar to the increase in CYP1A1 content (Fig. 2b). To see if we have the same effect in TNBC, we repeated the experiment using two TNBC cells, MDA-MB-468 and Hs578T. Suppl. Fig. 1 shows that TCDD and DMBA increased the BCL-2 and p-BCL-2 cellular contents similar to MCF-7 cells.

In vivo, IHC analysis of breast tissues from female Swiss albino mice treated with DMBA 30 mg/kg IP twice for one month (DMBA) or until the development of breast tumor (Tumor) showed higher expression levels of CYP1A1 and BCL-2 as compared with normal mammary gland (Fig. 2c), which was higher in DMBA-induced breast tumor samples than in DMBA-treated mice.

Effect of AhR/CYP1A1 pathway inhibition on the expression of BCL-2 in vitro and in vivo models

To directly examine the crosstalk between BCL-2 protein regulation and AhR/CYP1A1 pathway, we questioned whether blocking of AhR/CYP1A1 pathway using either genetic silencing by shRNA or pharmacological inhibitor would downregulate the expression and activity of BCL-2. Fig. 3 shows that silencing of AhR or CYP1A1 in MCF-7 cells significantly downregulated the expression of both total BCL-2 and p-BCL-2 (ser70) at both the flow cytometric (Fig. 3a) and mRNA (Fig. 3b) levels. This was further confirmed in the *in vivo* female Swiss albino mice model, where blocking of the AhR/CYP1A1 by α-NF (60 mg/kg) caused a dramatic decrease in BCL-2 IHC staining level (Fig. 3c). We further explored this crosstalk by investigating the impact of AKT, an AhR-regulated protein, on BCL-2 expression in response to DMBA. Treatment of MCF-7 cells with LY294002 (10 μM), an AKT pathway inhibitor, diminished the DMBA-induced upregulation of BCL-2 and p-BCL-2 cellular contents (Fig. 3d).

Effect of AhR/CYP1A1 inhibition on BCL-2 induction by chemotherapy and stemness

To examine whether chemotherapy-induced BCL-2 expression in breast cancer is also mediated through activation of the AhR/CYP1A1 pathway, independent serial experiments were conducted to test this hypothesis. First, treatment of MCF-7 cells with AhR/CYP1A1 inhibitor, α-NF (10 μM), followed by doxorubicin (DOX, 500 ng/ml) for an additional 48 h abrogated both basal and DOX-induced BCL-2 cellular contents and localization of both total and active form by IF (Fig. 4a). Second, genetic shRNA inhibition of AhR or CYP1A1 in MCF-7 cells treated with increasing concentrations of DOX (0, 250, and 500 ng/ml) significantly decreased the basal and DOX-induced BCL-2 protein expression levels, which was pronounced more by shRNA CYP1A1 (Fig. 4b). Third, inhibition of the AhR pathway decreased the DOX-induced CSC stemness

marker (SP). Fig. 4c shows that pretreatment of MCF-7 cells with AhR/CYP1A1 inhibitor Resveratrol (RES, 10 μM) in the presence and absence of DOX (500 ng/ml) significantly inhibited the percentage of basal and DOX-induced expansion of SP cells (80%) compared to the control level (Fig. 4c).

Effects of BCL-2 inhibition on AhR/CYP1A1 pathway and CSC expansion and chemoresistance

To further understand the crosstalk between AhR/CYP1A1 and BCL-2 pathways, we tested whether blocking of BCL-2 by VCX would inhibit the AhR-induced CSC features, such as mammospheres formation and percentage of SP. Pretreatment of MCF-7 (Fig. 5a) and Hs578T (Suppl. Fig. 1c) cells with the BCL-2 inhibitor VCX (10 μM) in the presence and absence of an AhR inducer, TCDD (10 nM) or DMBA (5 μM), significantly decreased the basal and TCDD- or DMBA-inducible CSC mammospheres formation by approximately 60% and 50%, respectively. Similar pattern was also observed in TNBC Hs578T cells (Suppl. Fig. 1c). Additionally, pretreatment of MCF-7 (Fig. 5b), MDA-MB-468, and Hs578T cells (Suppl. Fig. 2a) with VCX significantly blocked the increase of the percentage of SP cells in response to DOX in a concentration-dependent manner (Fig. 5b).

Next, we further examined whether activating the AhR/CYP1A1 pathway would sensitize CSCs to the apoptotic effects of VCX by staining the cells with CSCs marker CD44 and CD24, followed by apoptosis marker annexin-V. Flow cytometric analysis (Fig. 5c) shows that pretreatment of MCF-7 cells with TCDD sensitized CD44^{High}/CD24^{Low} cells to the apoptotic effects of VCX by two folds; however, no sensitization was observed with DOX treatment. The combination of DOX and VCX on TCDD-treated cells significantly induced massive apoptosis in CSCs by 14-fold. These results demonstrate that activation of the AhR/CYP1A1 pathway leads to a shift in the survival dependency of CSCs toward BCL-2.

Effect of BCL-2 inhibition by VCX treatment on mammary epithelial cell differentiation in vitro and in vivo models

In this experiment, we assessed the effect of the treatment of HMLE cells with increasing concentrations of VCX (1, 5, and 10 μM) for 72 h on mammary epithelium cell hierarchy and differentiation markers by flow cytometry. Results showed that HMLE cells in our culture method comprised a dominant cell population with a basal-like phenotype fitted in EpCAM^{Low}/CD49f^{High} combined with CD44^{High}/CD24^{Low} (Fig. 6a). Surprisingly, VCX treatment caused a significant increase in the luminal marker EpCAM and a decrease in basal marker CD49f, in a concentration-dependent manner. Interestingly, this change was accompanied by a reduction in CD44^{High}/CD24^{Low} phenotype population and an increase in CD44^{Low}/CD24^{High} phenotype population, which is a phenotype associated with a luminal differentiation state.

However, due to the complex nature of basal-luminal equilibrium and epithelium cell differentiation, it is challenging to draw a conclusion based on *in vitro* model. Thus we utilized *in vivo* model, in which female Swiss albino mice were treated with a single dose of VCX (30 mg/kg) every week for three weeks cycle. The mice were then sacrificed, and mammary glands were isolated for the preparation of MECs. Flow cytometry analysis of MECs lineage markers in mock mice using EpCAM and CD49f showed three populations that comprised the mammary gland, including basal, luminal, and stromal cells (Fig. 6b). Additional markers, including CD201 and CD61, were also used to distinguish the mammary stem cells in the basal-like EpCAM^{High}/CD49f^{High} population and luminal progenitor cells within luminal-like EpCAM^{High}/CD49f^{Low} population, respectively. The *in vivo* BCL-2 inhibition by VCX treatment
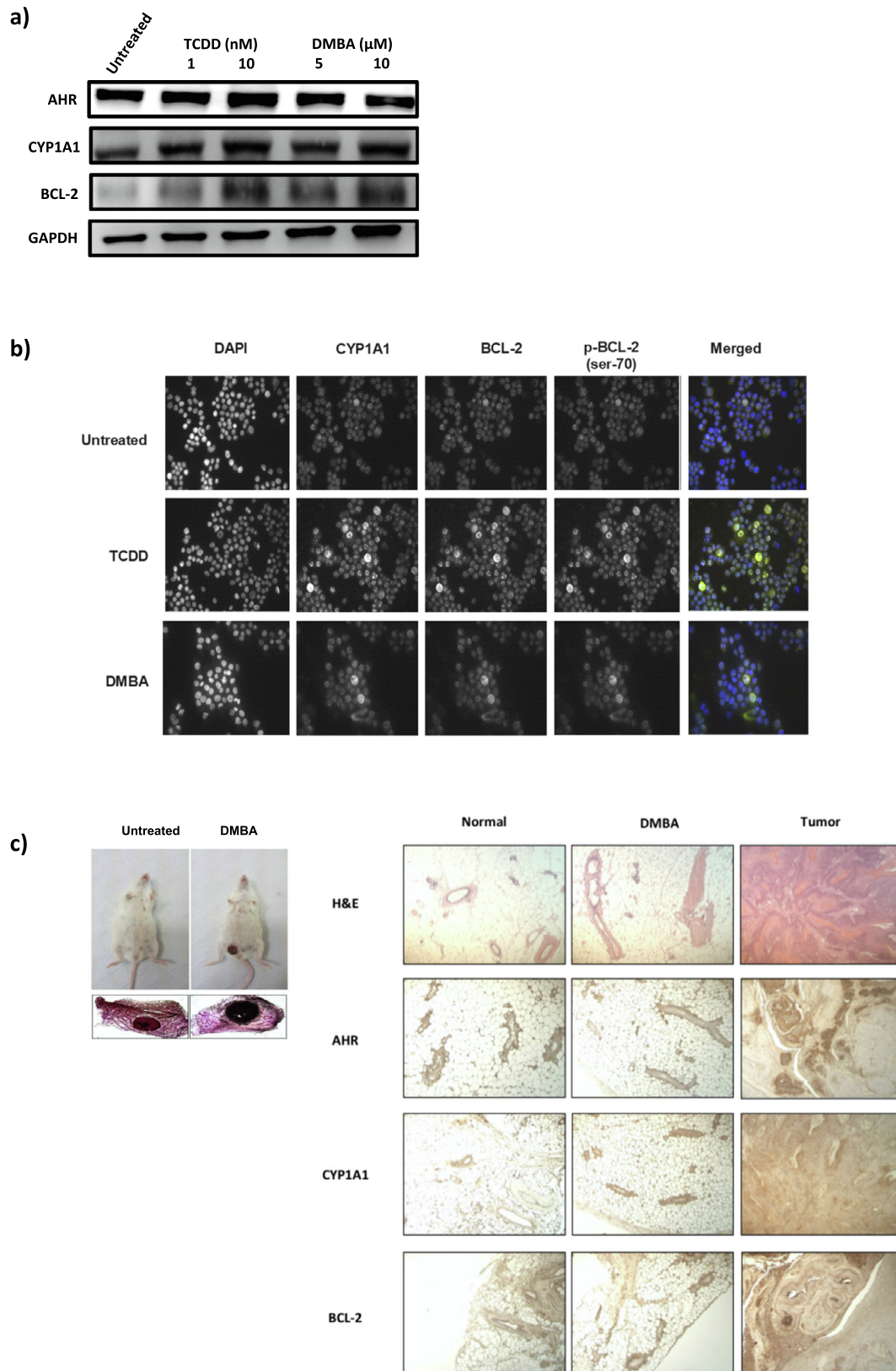
Fig. 2. Basal and inducible expression of BCL-2 *in vitro* and *in vivo* models. a) MCF-7 cells were treated with either TCDD (1 and 10 nM) or DMBA (5 and 10 µM) for 24 h, thereafter protein expression levels of the target genes were determined by Western blot analysis. **b)** MCF-7 cells were treated for 48 h with either TCDD (10 nM) or DMBA (5 µM), thereafter, CYP1A1, BCL-2, and p-BCL-2 protein cellular content and localization were conducted by IF. **c)** Female Swiss albino mice were treated with DMBA 30 mg/kg IP twice for one month and the physical apparent/morphology of both normal and DMBA-induced breast tumors and the expression of the target genes were determined by IHC.
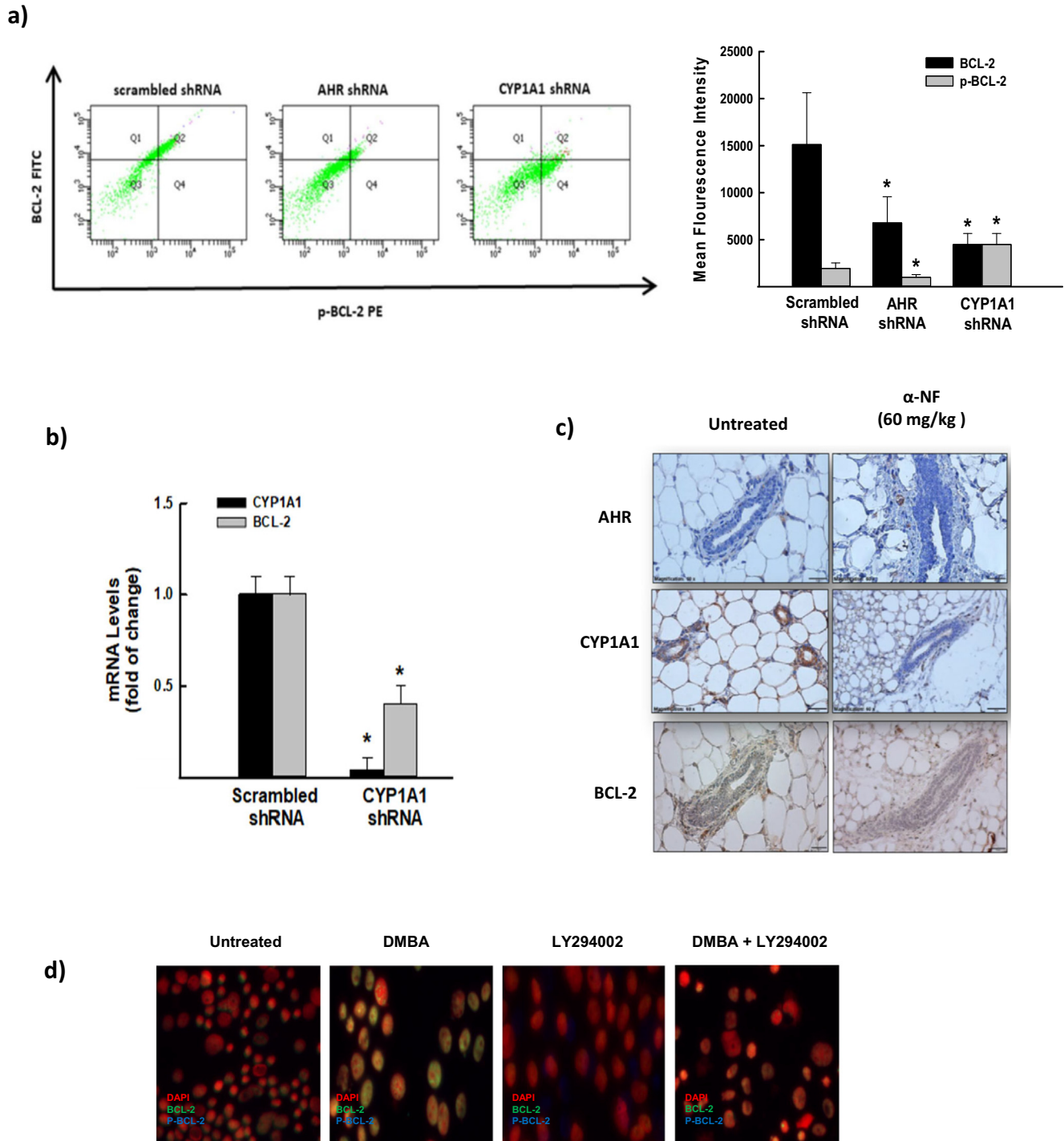
A. Al-Dhfyan, A. Alaiya, F. Al-Mohanna et al.

Fig. 3. Constitutive and inducible expression of BCL-2 in breast tumors in mice and MCF-7 cells. MCF-7 cells were transfected with shRNA against either AhR or CYP1A1; thereafter, **a)** BCL-2 and p-BCL-2 protein expression levels were determined by flow cytometry, and **b)** mRNA expression levels of BCL-2 and CYP1A1 were quantified by RT-PCR. **c)** Female Swiss albino mice were treated with AhR inhibitor α-NF 60 mg/kg IP twice for one month; thereafter, AhR, CYP1A1, and BCL-2 protein expression levels were determined by IHC. **d)** MCF-7 cells were pretreated with LY294002 followed by DMBA for 24 h and the BCL-2 and p-BCL-2 . Cellular contents and localization were determined by IF. The values are presented as the mean of fold change ± SEM (n = 6) in triplicate. *; p < 0.05 compared to control shRNA (student's t-test).

showed a significant increase in the luminal-like cells population, similar to the *in vitro* study. Furthermore, a substantial increase in the CD61⁺ population within the luminal-like population was detected; however, no significant increase in basal-like or mammary stem-like cells was seen (Fig. 6b).

Effect of long-term VCX treatment on epithelial to mesenchymal transmission (EMT)

The VCX's potential to induce dedifferentiation of luminal cells prompted us to explore further the effect of VCX on epithelial-
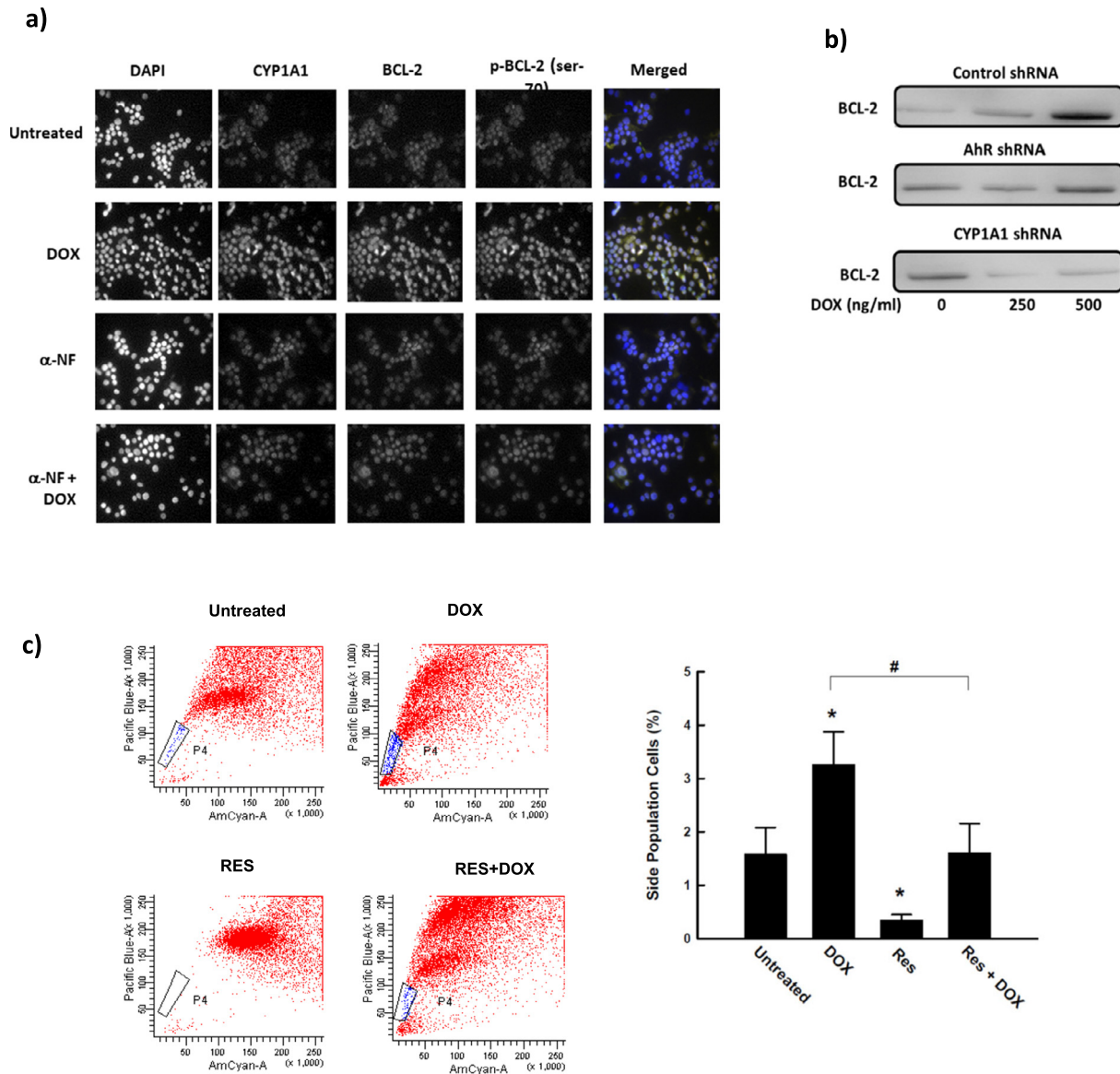
Fig. 4. Effect of AhR/CYP1A1 inhibition on BCL-2 induction by DOX. a) MCF-7 cells were pretreated for 2 h with α-NF (10 μM), followed by DOX (500 ng/ml) for 48 h; thereafter, the localization and cellular content of CYP1A1, BCL-2, and p-BCL-2 were measured by IF. **b)** MCF-7 cells were transfected with either shRNA AhR or CYP1A1 in the presence of DOX (250 and 500 ng/ml) for 48 h. Thereafter, BCL-2 protein expression level was determined by Western blot analysis. **C)** MCF-7 cells were treated for 72 h with DOX (500 ng/ml) and RES (10 μM). The percentage of SP cells was then determined using an LSRII® flow cytometer. The values are presented as the mean of fold change ± SEM (n = 6) in triplicate. *; $p < 0.05$ compared to control (untreated), #; $p < 0.05$ compared to DOX treatment (ANOVA followed by Student–Newman–Keul's test post hoc).

mesenchymal transition (EMT). First, long-term treatment of HMLE cells with VCX (1 μM) for two weeks induced changes in the morphological structure of the cells characterized by a lack of clustering of cells that make epithelial-like islands (Fig. 7a). Therefore, we sought to link this morphological change with EMT by determining the cellular contents and localizations of EMT markers (vimentin and E-cadherin) and epithelial lineage markers (CK18 and p63) using IF. Consistency with morphological transition, long-term VCX treatment induced EMT, as evidenced by induced the mesenchymal marker, vimentin, and reduced the epithelial marker, E-cadherin. Furthermore, the EMT-induced cells were absent of luminal and basal lineage markers, p63 and CK18 (Fig. 7b).

To confirm the effect of VCX on luminal/basal cell differentiation, we examined the effect of VCX onset on transcriptional factors involved in the luminal differentiation of MECs, such as GATA-3 and Slug. Fig. 7c shows that VCX (1 μM) treatment of

HMLE cells did not affect GATA-3 cellular contents, but modulated Slug content. Furthermore, we linked the effect of VCX on EMT with the AhR levels by measuring the impact of VCX on AhR activity using IHC and IF in both in vivo and in vitro cells. As Fig. 7d illustrates, breast tissues isolated from Swiss albino mice treated with VCX (30 mg/kg) (IP) once a week for two cycles exhibited increased IHC staining of AhR. Similarly, VCX-treated HMLE cells showed a marked increase in AhR cellular content and localization. Because of the association between EMT and tumor formation, we sought to measure the tumorigenic potential of EMT clone cells and compared them with untreated counterparts. Therefore, one million viable cells of untreated and VCX-treated cells were mixed with Matrigel 1:1 DMEM/F12 and injected into the same immunocompromised nude mice (n = 4) on both sides. Mice treated with VCX failed to develop breast tumors after observation for 12 weeks on the VCX injection side, as shown in Fig. 7e.
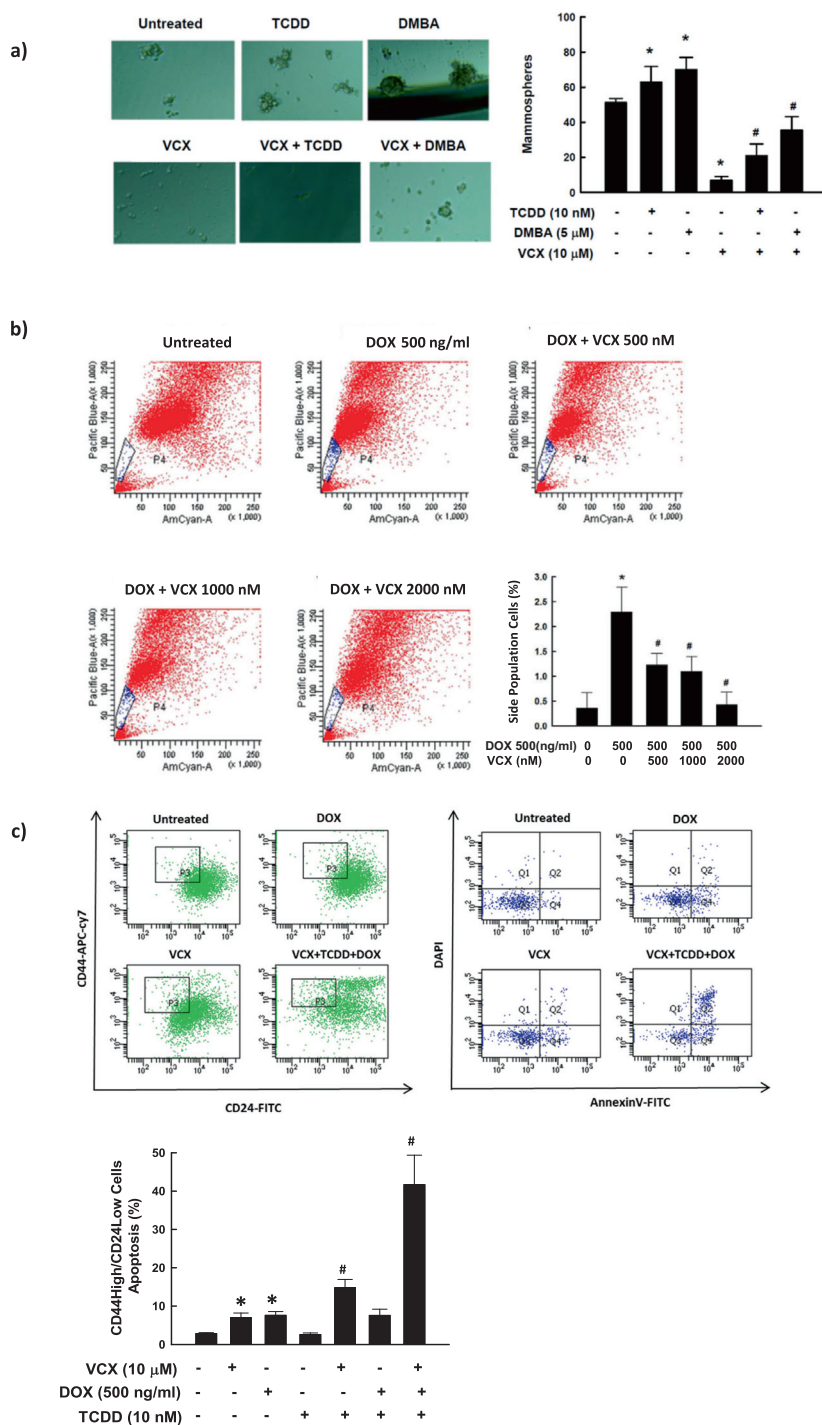
A. Al-Dhfyan, A. Alaiya, F. Al-Mohanna et al.

Fig. 5. **Effect of BCL-2 inhibition by VCX on the AhR/CYP1A1-mediated CSC expansion and chemoresistance. a)** MCF-7 cells were treated with TCDD (10 nM) or DMBA (5 μM) in the presence and absence of VCX (10 μM). After that, the mammosphere numbers and size were determined by Evos® transmitted light microscope. The values are presented as the mean of fold change ± SEM (n = 3) in triplicate. *; p < 0.05 compared to control (untreated), #; p < 0.05 compared to corresponding treatment in the absence of VCX (ANOVA followed by Student–Newman–Keul's test post hoc). **b)** MCF-7 cells were treated with DOX (500 ng/ml) in the presence and absence of three concentrations of VCX (500, 1000, and 2000 nM). Thereafter, the percentage of SP cells was determined using a Lan SRII® flow cytometer. The values are presented as the mean of fold change ± SEM (n = 3) 0.05 compared to control (untreated), #; p < 0.05 compared to DOX alone treatment (ANOVA followed by Student–Newman–Keul's test post hoc). **c)** MCF-7 cells were treated with DOX (500 ng/ml) or VCX (10 μM) or a combination in the presence of TCDD (10 nM). The CD44 and CD24 positive and apoptosis cells were determined by flow cytometry. Duplicate reactions were performed for each experiment. The values are presented as the mean ± SEM (n = 3). *; p < 0.05 compared to control (untreated), #; p < 0.05 compared to VCX alone treatment (ANOVA followed by Student–Newman–Keul's test post hoc).

In silico VCX reactivity and toxicity prediction

The accumulation of experimental evidence of VCX toxicity on MECs prompted us to evaluate the theoretical toxicity predictions based on computational methods for estimating the toxicity of VCX using the reactivity module in the Xenosite web page, Sarah, and DEREC models. Sarah's model results indicate that VCX is expected to show *in vitro* mutagenicity, as it is predicted to be positive in a
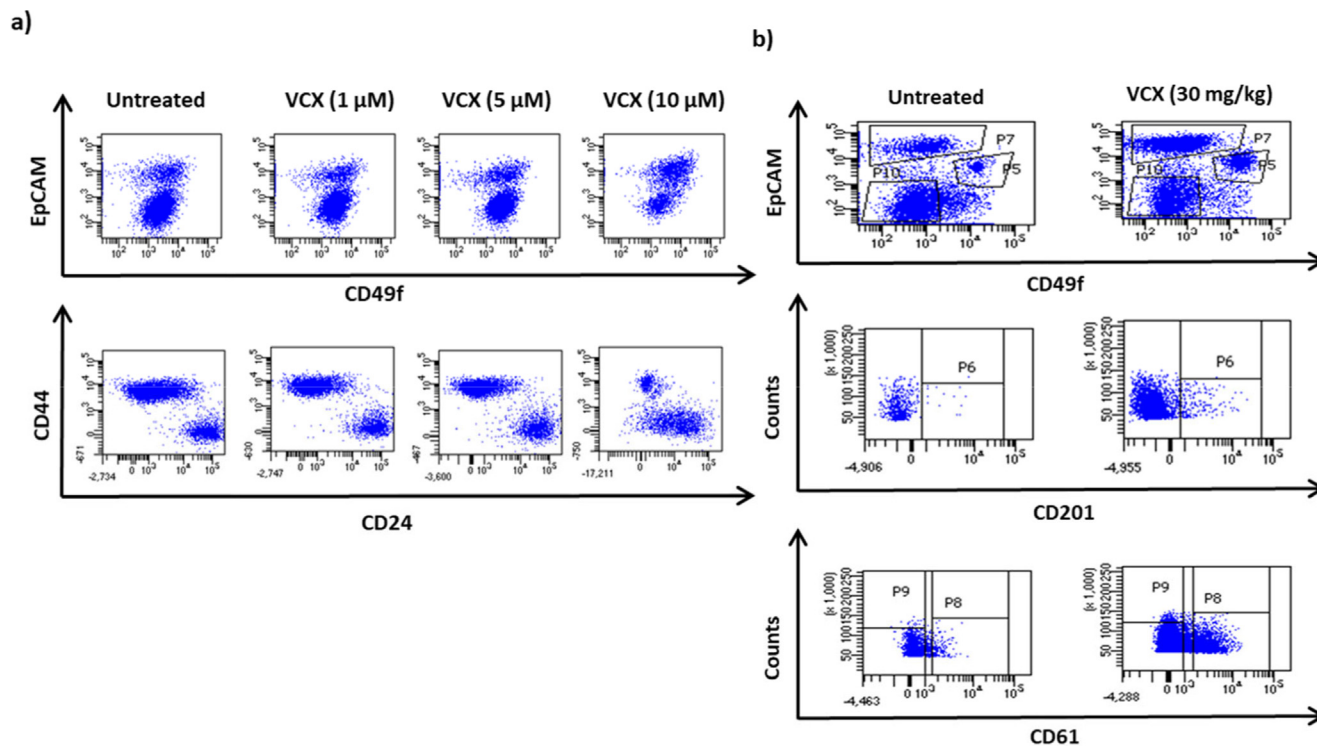
Fig. 6. Effect of VCX treatment on epithelial cell population and breast cancer stemness marker. a) HMLE cells were treated with VCX (1, 5, and 10 µM) after that, the cell population with a basal-like phenotype EpCAM/CD49f and CD44^High/CD24^Low were determined by flow cytometry. **b)** Female Swiss albino mice were treated with VCX (30 mg/kg) each week for a 3-week cycle where the females were sacrificed, and mammary glands taken on the last day of the 4th-week period were then prepared for detection of the MECs lineage markers EpCAM, CD49f, CD201, CD61 by flow cytometry.

bacterial reverse mutation assay (Ame's test), a widely used test to detect mutagens. The Derek Nexus prediction reveals that VCX shows structural alerts, including aryl sulfonamide that causes urothelial bladder hyperplasia and other organ toxicities. In addition, the presence of an aromatic nitro group in VCX structure is known to mediate carcinogenicity, chromosome damage, mutagenicity, and HERG Pharmacophore I which causes HERG channel inhibition (plausible) (Fig. 8a). Importantly, the tetrahydropyran and piperazine rings are expected potential atomic sites for the bioactivation and cyanide attack in the VCX chemical structure. No GSH bioactive center was detected. Sulphonamide and aromatic nitro groups are predicted to play a role in VCX reactivity, causing DNA and protein damage (Fig. 8b).

To further assess the safety of VCX in humans, specifically its potential to induce breast cancer, we examined the FDA Adverse Event Reporting System (FAERS) database for any breast cancer cases reported with the use of VCX. FEARS database showed 15 breast cancer cases (Fig. 8C) that were reported from 2017 to March 2022. Most cases are breast cancer 12 (80%), two cases of breast cancer with metastasis (13.3%), and one case of recurrent breast cancer (6.7%). Most of the reported breast cancer cases are above 65 years (93.3%), 60% were reported in the USA, while 40% of the cases were reported in Europe (Fig. 8C).

Effect of AhR inhibition on VCX-induced mammary epithelium cells differentiation abnormality

The results presented in Figs. 7 and 8 raised the question of whether the AhR/CYP1A1 pathway plays a role in VCX-induced EMT. To address this question, we examined whether inhibition of AhR would protect against VCX-induced MEC dedifferentiation. For this purpose, BALB/C female mice were treated with a single dose of VCX (30 mg/kg) every week for two weeks cycle in the

presence and absence of an AhR inhibitor, either α-NF (60 mg/kg) or MET (40 mg/kg) (Suppl. Fig. 2b). MECs were then isolated after one and three weeks post-treatment and prepared as single-cell suspensions for further analysis on a FACS LSRII (BD Biosciences) using cell differentiation markers. As illustrated in Fig. 9a and b, VCX treatment increased EpCAM^High/CD49F^Low CD61^+ luminal progenitor-like cells by 14.4% and 11.5% compared to 6.7% and 5.8% for normal untreated mice in 1st- and 3rd-week post-treatment, respectively. However, co-treatment with either α-NF or MET inhibited the increase in EpCAM^High/CD49F^Low CD61^+ luminal progenitor by 3.4% and 10% in 1st-week post-treatment and by 8.8% and 8.3% in 3rd-week post-treatment, respectively. Fig. 9a and b show that the VCX-mediated increase of the EpCAM^High/CD49f^Low CD61^+ (luminal progenitor-like cells) was significantly blocked by both AhR inhibitors, α-NF and MET. However, we found that after three weeks, AhR direct antagonist α-NF, which prevents the translocation of AhR to the nucleus as shown in Fig. 4c, severely affected the mammary gland branching and inducible level of EpCAM^High/CD49f^High CD201^+ (mammary epithelial system-like cells (Fig. 9b).

To further confirm the protective effect of the AhR inhibitor, we measured additional lineage-specific markers: CK18 and p63, for luminal epithelial cells in mammary gland tissues of mice treated with VCX in combination with either α-NF or MET. Fig. 10 shows that cellular changes of epithelial and luminal cell markers, CK18 and p63, by VCX were corrected by co-administration with AhR antagonists, α-NF, and MET.

Discussion

Several recent studies have reported that activation of AhR dramatically increased CSCs development and characteristics using *in vitro* human cell lines and *in vivo* animal models of breast cancer
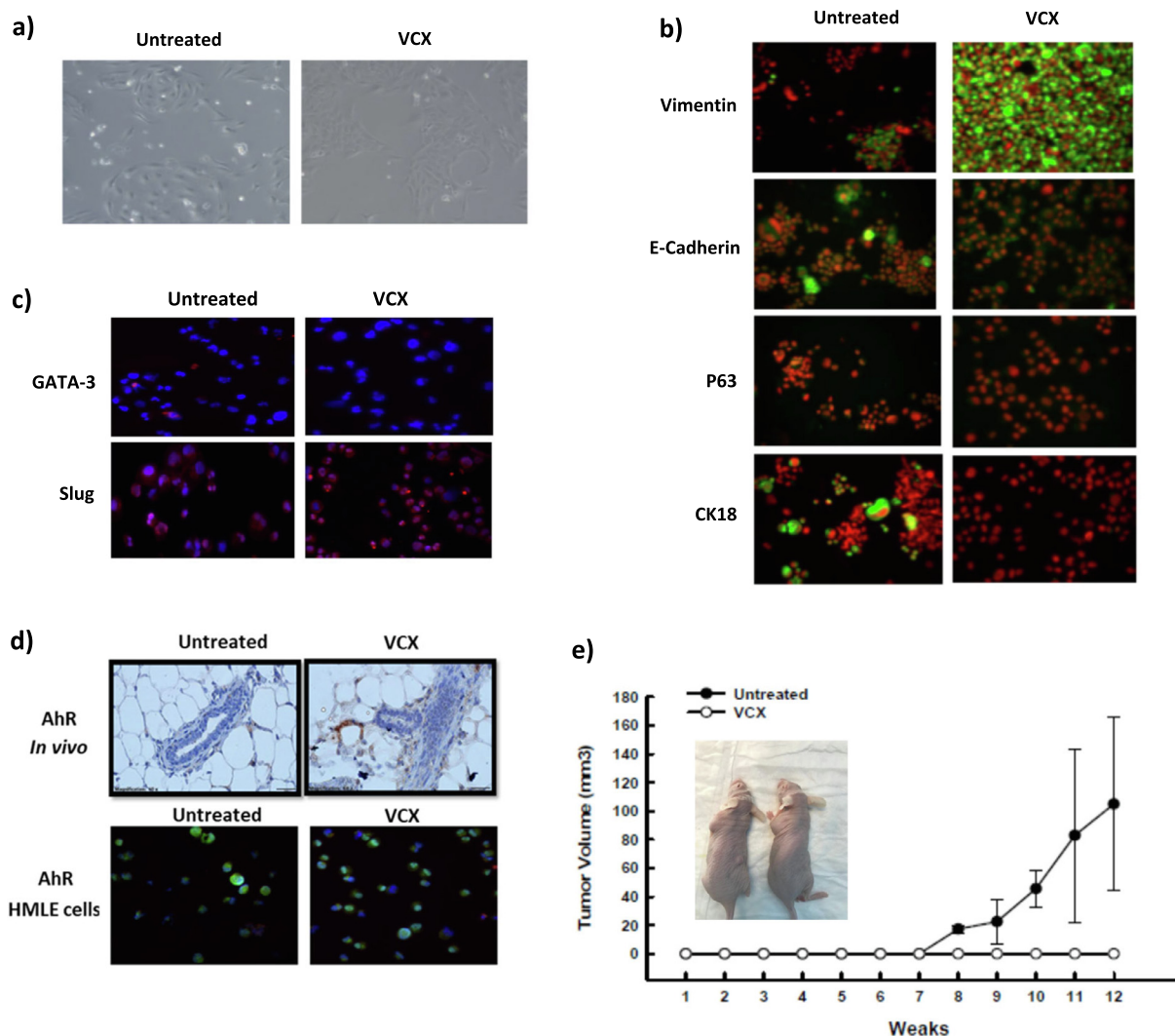
Fig. 7. Effect of long-term treatment with VCX on cell EMT. HMLE cells were treated with VCX (1 µM) for two weeks, and thereafter **a)** the changes in the morphological structure of the cells and **b)** vimentin, E-cadherin, CK18, and p63, and **c)** proteins involved in the differentiation MECs, GATA-3 and Slug were determined by IF. **d)** AhR expression was determined in female Swiss albino mice treated with VCX (30 mg/kg) for once a week for two cycles by IHC and in HMLE cells treated with VCX (1 µM) for 72 h by IF. **e)** Female 6-week-old nude mice were injected with control or VCX-treated HMLE cells. The tumor volume was measured with a caliper and calculated using; tumor volume (V) = 1/2 (width^2 × length).

[6,7,28]. These studies show that CSCs exhibit higher expression and activity levels of CYP1A1 than non-CSCs, differentiated cells, and that overexpression of AhR/CYP1A1 promoted CSC proliferation and chemoresistance through the activation of the Wnt/β-catenin pathway [6]. Several pieces of evidence support the concept that distinct subtypes of cancers within an organ may originate from different cells knowns as cells of origin [29]. Identifying these target breast cells will help in the earlier detection of malignancies and may lead to preventive therapies. In the context of the cell of origin and DMBA-induced breast tumor *in vivo*, we questioned what cell of origin was first targeted by DMBA and culminated in cancer initiation. Mammary breast cell profiling analysis, using a well-established flow cytometric markers for mouse breast cells sub-populations, indicated that DMBA-induced tumor is a luminal originate and luminal progenitor cells (EpCAM^{High}/CD49f^{Low} CD61$^+$) [36]. These results encouraged us to further understand the molecular mechanisms to identify novel proteins for possible drug targeting. For this aim, proteomics analysis of the proteome of MCF-7 cells treated with AhR inducer showed significant changes in global protein expression profiles of approximately 1553 proteins. Interestingly, BCL-2 protein

showed the highest inducible protein in response to the AhR inducer linked to cancer proliferation and cell cycle. Similar results from our laboratory have shown that TCDD induces several anti-apoptotic proteins such as BCL-xl and MCL-1 in ovarian cancer cell lines [37].

The BCL-2 protein family is commonly expressed in several human cancer types where its expression is associated with an aggressive disease course and poor survival [30]. The overexpression of BCL-2 has been reported in ∼ 75% of breast cancer cases and thus has emerged as an important prognostic marker [15]. Although several studies have linked BCL-2 expression and the survival rate in breast cancer patients [30], how BCL-2 could function as a therapeutic target for breast cancer is not concrete. The crosstalk between the BCL-2 and AhR/CYP1A1 pathways in breast cancer and CSCs development is supported by several observations. First, the activation of the AhR/CYP1A1 pathway *in vitro* MCF-7, Hs578T, MDA-MB-486, and HMLE cells and *in vivo* mouse models resulted in significant and proportional increases in BCL-2 and p-BCL-2 proteins cellular content. Second, chemical inhibition and silencing of AhR/CYP1A1 markedly downregulated the expression of BCL-2 levels in both *in vitro* human cancer cells and *in vivo*
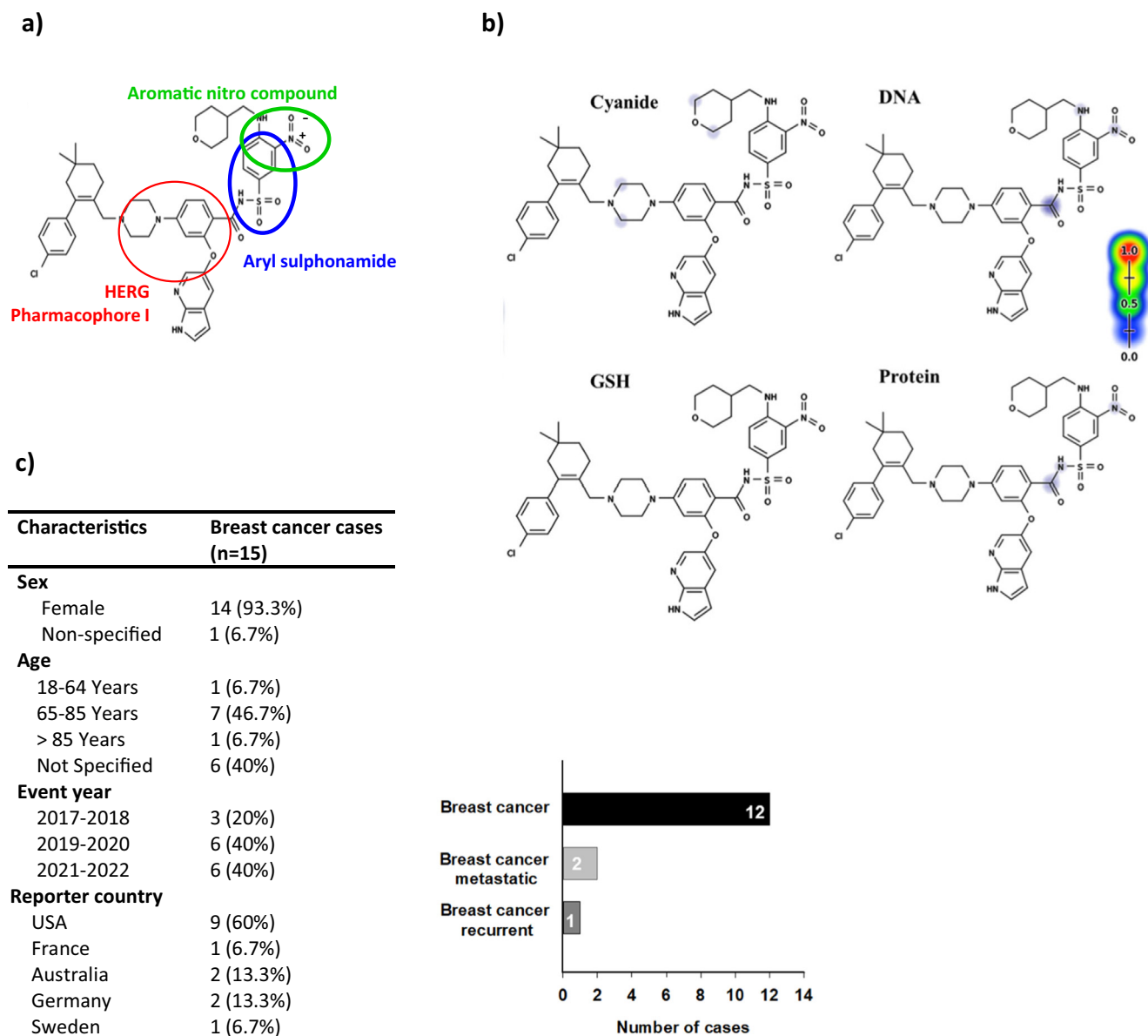
a)

b)

c)

Characteristics	Breast cancer cases (n=15)
Sex	
Female	14 (93.3%)
Non-specified	1 (6.7%)
Age	
18-64 Years	1 (6.7%)
65-85 Years	7 (46.7%)
> 85 Years	1 (6.7%)
Not Specified	6 (40%)
Event year	
2017-2018	3 (20%)
2019-2020	6 (40%)
2021-2022	6 (40%)
Reporter country	
USA	9 (60%)
France	1 (6.7%)
Australia	2 (13.3%)
Germany	2 (13.3%)
Sweden	1 (6.7%)

Fig. 8. In silico prediction of VCX reactivity. a) Structural alerts of VCX. **b)** Predicted bioactive sites of VCX showing DNA, GSH, protein, and cyano bioactive centers. dark blue reveals high probability for these groups to form reactive intermediates, whereas faint blue reveals less probability. **c)** Breast cancer incident cases reported with VCX use and the demographic data were extracted from FEARS databases. (For interpretation of the references to colour in this figure legend, the reader is referred to the web version of this article.)

mouse models, which was accompanied by a decrease in CSC features. In agreement with our observations, it has been reported that AhR activation by TCDD mediates apoptosis [31,32] and that silencing of CYP1A1 in prostate cancer cells downregulates BCL-2 levels [33].

Venetoclax (VCX) is one of these promising BCL-2 inhibitors that received accelerated FDA approval in the United States as a monotherapy for patients with chronic lymphocytic leukemia [34]. With increased BCL-2 expression, breast cancer may respond to VCX therapy, and thus we thought to examine the therapeutic effect of VCX on breast CSCs and the role of AhR. In this study, the direct involvement of BCL-2 in breast CSC expansion was proven by the ability of VCX to a) block the basal and AhR/CYP1A1-mediated breast CSCs development and b) prevent tumor formation ability in immune-deficient mice. Surprisingly, we report here the first observations that long-term treatment of HMLE cells with VCX alone induced changes in the morphological structure of the

cells with an increase in luminal-like cell population and a decrease in epithelial markers. This luminal dedifferentiation state by VCX is attributed to the potential of VCX to a) induce EMT characterized by increased mesenchymal marker, vimentin, and decreased epithelial marker, E-cadherin, b) induce Slug expression, a transcription factor involved in luminal differentiation of MECs, and c) increase the expression of AhR *in vitro* and *in vivo* models. The cell dedifferentiation effect of VCX raises the question of whether VCX has a cytotoxicity effect. This question was addressed by conducting *in silico* toxicity assessment, which showed the reactivity of sulphonamide and aromatic nitro groups of VCX structure toward DNA and protein with electrophiles, i.e., cyanide and glutathione. Additionally, *in silico* toxicity prediction software (Sarah Nexus and Derek Nexus) demonstrated that VCX exhibits mutagenicity attributed to the aromatic nitro group. These observations are supported by the FEARS pharmacovigilance database, which
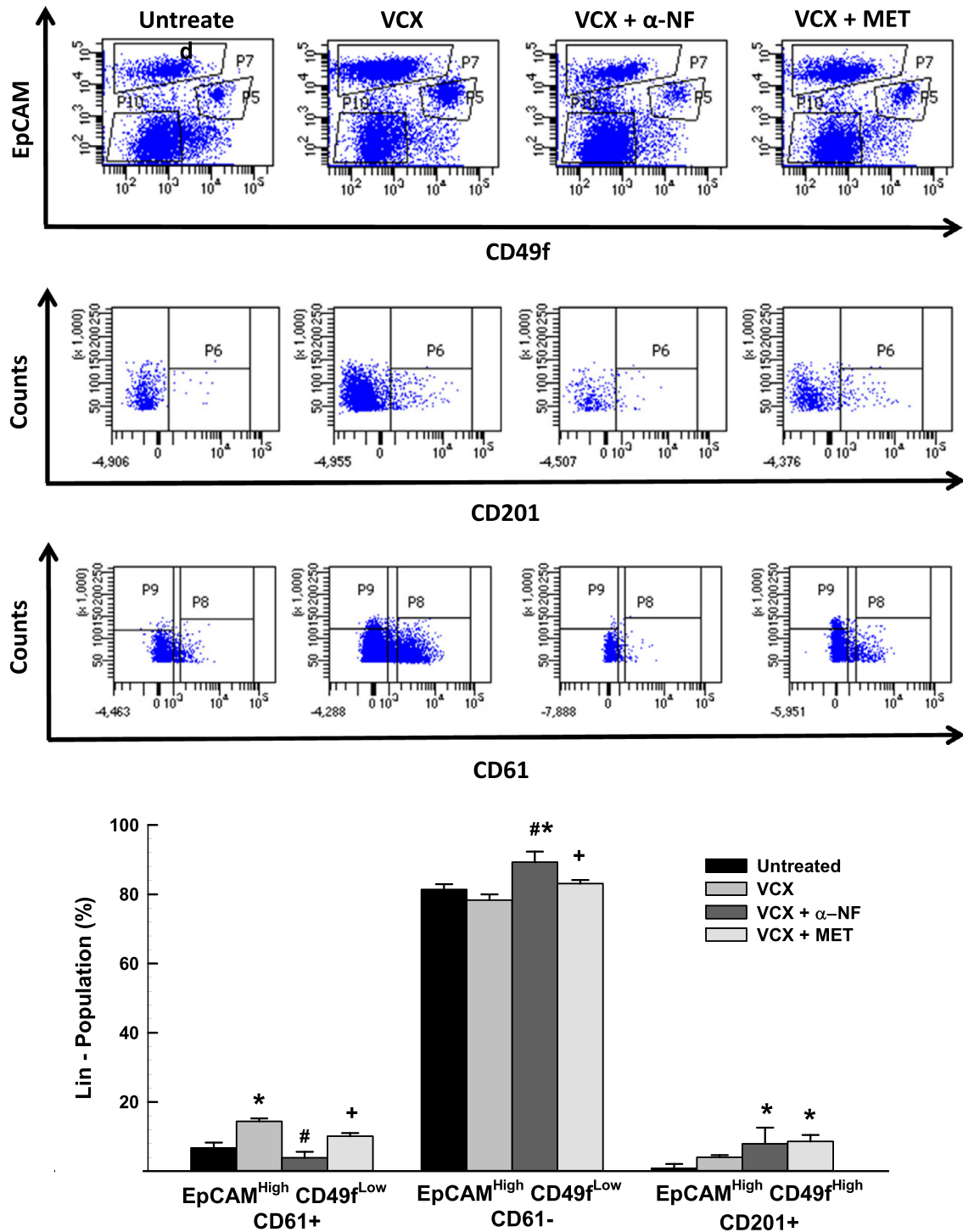
A. Al-Dhfyan, A. Alaiya, F. Al-Mohanna et al.

a) 1st Week post treatment

Fig. 9. The effect of AhR/CYP1A1 inhibition on VCX-induced MECs differentiation abnormality. Female BALB/C mice were treated with VCX (30 mg/kg) alone or in combination with either α-NF (60 mg/kg) or MET (40 mg/kg)**a)** one week or **b)** three weeks post-treatment. After that, mice were sacrificed, and mammary glands taken in the last were prepared to determine the epithelial cell lineage markers EpCAM, CD49f, CD201, and CD61 by flow cytometry. The values are presented as the mean ± SEM (n = 3). *; $p < 0.05$ compared to control, #; $p < 0.05$ compared to VCX alone treatment (ANOVA followed by Student–Newman–Keul's test post hoc).
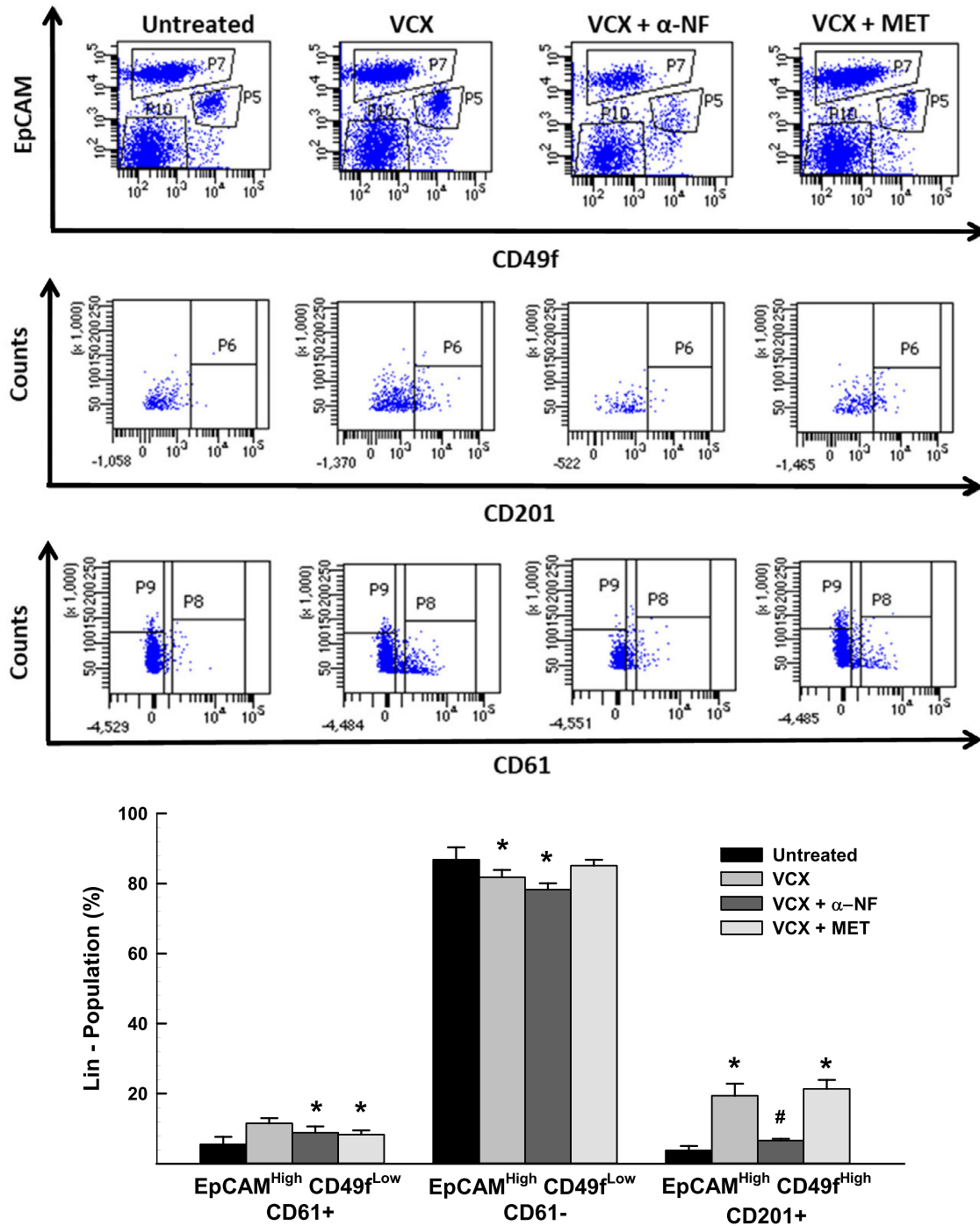
b) 3rd Week post treatment

Fig. 9 (*continued*)

reported fifteen breast cancer cases with VCX treatment from 2017 to Mar 2022 [27].

In the current study, the observations that VCX alone induced AhR and activated EMT while inhibited AhR-induced cancer progression and CSC chemoresistance, in addition to the FDA FEARS data encouraged us to further test whether combining VCX with AhR antagonist would protect against VCX mammary cell dedifferentiation. For this purpose, we tested the effect of two different AhR antagonists; α-NF, which is an AhR ligand that prevents the translocation of AhR to the nucleus and hence inhibits AhR activation directly, and MET, which does not bind to AhR but inhibits xenobiotic responsive element luciferase reporter gene and hence inhibits AhR activation indirectly [35]. Perhaps the most interesting finding in this study is the observation that the combination of either α-NF or MET with VCX significantly inhibited luminal progenitor-like cells in the short term. However, long-term treat-
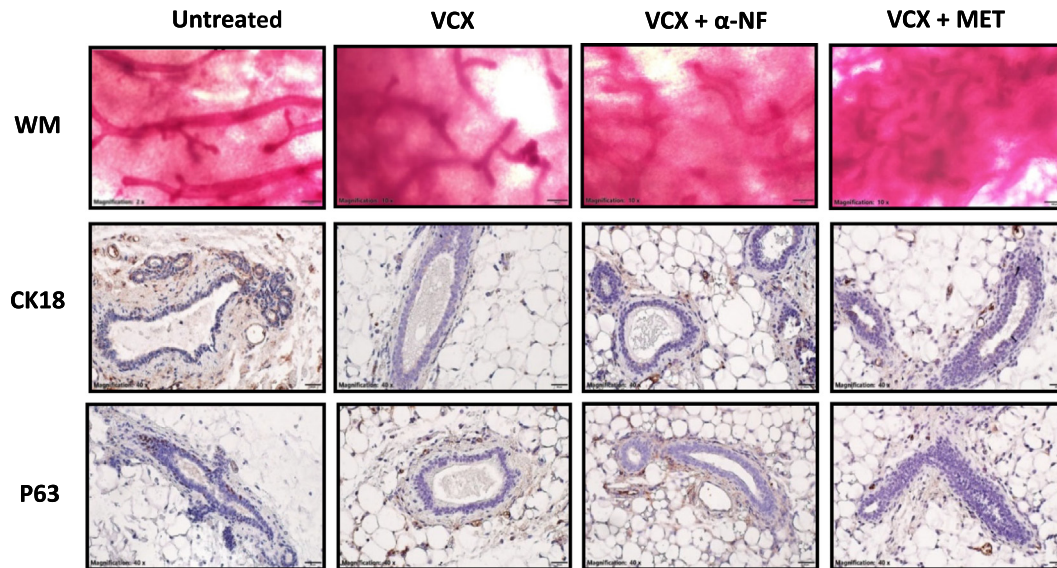
Fig. 10. The protective effect of AhR inhibitor combination with VCX on epithelial and luminal cell markers. Mammary gland whole mounts and mammary lineage markers p63 and CK18 from female BALB/C mice treated with VCX (30 mg/kg) alone and in combination with either α-NF (60 mg/kg) or MET (40 mg/kg) for three weeks were determined by IHC analysis.

ment with the direct AhR antagonist α-NF severely affects mammary gland branching and the inducible level of the mammary epithelial stem-like cells. Therefore, further studies are needed to explore the VCX and MET combination effect in treating breast cancer.

Conclusion

This study provides the first evidence that breast CSC expansion and chemoresistance by the AhR/CYP1A1 are BCL-2-dependent effects. Identification of the BCL-2 protein as a druggable downstream target of the AhR/CYP1A1 signaling pathway will establish a basis for efficient therapeutic strategies to target CSCs and chemoresistance, supporting the rational use of BCL-2 inhibitors for treating breast cancer. The study also recommends a combination of VCX with MET for better breast cancer treatment and toxicities. Clinical trials are warranted to examine the clinical impact of combined BCL-2 and AHR inhibitors on breast cancer development, progression, and chemoresistance.

Compliance with ethics requirements

All Institutional and National Guidelines for the care and use of animals were followed.

CRediT authorship contribution statement

Abdullah Al-Dhfyan: Methodology, Formal analysis, Investigation, Writing – review & editing. **Abdulkareem Alaiya:** Conceptualization, Methodology, Writing – original draft. **Falah Al-Mohanna:** Methodology, Investigation, Writing – review & editing. **Mohamed W Attwa:** . **Abdullah F. Alasmari:** Supervision, Writing – review & editing. **Saleh A. Bakheet:** Supervision, Writing – review & editing. **Hesham M. Korashy:** Conceptualization, Investigation, Writing – review & editing, Supervision, Project administration, Funding acquisition.

Declaration of Competing Interest

The authors declare that they have no known competing financial interests or personal relationships that could have appeared to influence the work reported in this paper.

Appendix A. Supplementary data

Supplementary data to this article can be found online at https://doi.org/10.1016/j.jare.2022.10.006.

References

[1] McDermott SP, Wicha MS. Targeting breast cancer stem cells. Mol Oncol 2010;4(5):404–19.
[2] Li HZ, Yi TB, Wu ZY. Suspension culture combined with chemotherapeutic agents for sorting of breast cancer stem cells. BMC cancer 2008;8:135.
[3] Yu SC, Bian XW. Enrichment of cancer stem cells based on the heterogeneity of invasiveness. Stem cell reviews 2009;5(1):66–71.
[4] Dontu G, Al-Hajj M, Abdallah WM, Clarke MF, Wicha MS. Stem cells in normal breast development and breast cancer. Cell Prolif 2003;36(Suppl 1):59–72.
[5] Reya T, Morrison SJ, Clarke MF, Weissman IL. Stem cells, cancer, and cancer stem cells. Nature 2001;414(6859):105–11.
[6] Al-Dhfyan A, Alhoshani A, Korashy HM. Aryl hydrocarbon receptor/cytochrome P450 1A1 pathway mediates breast cancer stem cells expansion through PTEN inhibition and beta-Catenin and Akt activation. Mol Cancer 2017;16(1):14.
[7] Jung J-W, Park S-B, Lee S-J, Seo M-S, Trosko JE, Kang K-S, et al. Metformin represses self-renewal of the human breast carcinoma stem cells via inhibition of estrogen receptor-mediated OCT4 expression. PLoS ONE 2011;6(11): e28068.
[8] Kerzee JK, Ramos KS. Constitutive and inducible expression of Cyp1a1 and Cyp1b1 in vascular smooth muscle cells: role of the Ahr bHLH/PAS transcription factor. Circ Res 2001;89(7):573–82.
[9] Whitelaw ML, Gottlicher M, Gustafsson JA, Poellinger L. Definition of a novel ligand binding domain of a nuclear bHLH receptor: co-localization of ligand and hsp90 binding activities within the regulable inactivation domain of the dioxin receptor. Embo J 1993;12(11):4169–79.

A. Al-Dhfyan, A. Alaiya, F. Al-Mohanna et al.

[10] Pollenz RS. The mechanism of AH receptor protein down-regulation (degradation) and its impact on AH receptor-mediated gene regulation. Chem Biol Interact 2002;141(1–2):41–61.

[11] Whitlock JP. Induction of cytochrome P4501A1. Annu Rev Pharmacol Toxicol 1999;39(1):103–25.

[12] Shimada T, Fujii-Kuriyama Y. Metabolic activation of polycyclic aromatic hydrocarbons to carcinogens by cytochromes P450 1A1 and 1B1. Cancer Sci 2004;95(1):1–6.

[13] Buters JTM, Sakai S, Richter T, Pineau T, Alexander DL, Savas U, et al. Cytochrome P450 CYP1B1 determines susceptibility to 7,12-dimethylbenz[a] anthracene-induced lymphomas. Proc Natl Acad Sci USA 1999;96(5):1977–82.

[14] Bomken S, Fiser K, Heidenreich O, Vormoor J. Understanding the cancer stem cell. Br J Cancer 2010;103(4):439–45.

[15] Merino D, Lok SW, Visvader JE, Lindeman GJ. Targeting BCL-2 to enhance vulnerability to therapy in estrogen receptor-positive breast cancer. Oncogene 2016;35(15):1877–87.

[16] Youle RJ, Strasser A. The BCL-2 protein family: opposing activities that mediate cell death. Nat Rev Mol Cell Biol 2008;9(1):47–59.

[17] Juárez-Salcedo LM, Desai V, Dalia S. Venetoclax: evidence to date and clinical potential. Drugs Context 2019;8:1–13.

[18] Almozyan S, Colak D, Mansour F, Alaiya A, Al-Harazi O, Qattan A, et al. PD-L1 promotes OCT4 and Nanog expression in breast cancer stem cells by sustaining PI3K/AKT pathway activation. Int J Cancer 2017;141(7):1402–12.

[19] Wang R, Lv Q, Meng W, Tan Q, Zhang S, Mo X, et al. Comparison of mammosphere formation from breast cancer cell lines and primary breast tumors. J Thorac Dis 2014;6(6):829–37.

[20] Dontu G, Abdallah WM, Foley JM, Jackson KW, Clarke MF, Kawamura MJ, et al. In vitro propagation and transcriptional profiling of human mammary stem/progenitor cells. Genes Dev 2003;17(10):1253–70.

[21] Maayah ZH, Ansari MA, El Gendy MA, Al-Arifi MN, Korashy HM. Development of cardiac hypertrophy by sunitinib in vivo and in vitro rat cardiomyocytes is influenced by the aryl hydrocarbon receptor signaling pathway. Arch Toxicol 2014;88(3):725–38.

[22] Livak KJ, Schmittgen TD. Analysis of relative gene expression data using real-time quantitative PCR and the 2(-Delta Delta C(T)) Method. Methods 2001;25(4):402–8.

[23] Wetzig A, Alaiya A, Al-Alwan M, Pradez CB, Pulicat MS, Al-Mazrou A, et al. Differential marker expression by cultures rich in mesenchymal stem cells. BMC Cell Biol 2013;14(1).

[24] Korashy HM, El-Kadi AO. Differential effects of mercury, lead and copper on the constitutive and inducible expression of aryl hydrocarbon receptor (AHR)-regulated genes in cultured hepatoma Hepa 1c1c7 cells. Toxicology 2004;201(1–3):153–72.

[25] dos Santos CO, Rebbeck C, Rozhkova E, Valentine A, Samuels A, Kadiri LR, et al. Molecular hierarchy of mammary differentiation yields refined markers of mammary stem cells. Proc Natl Acad Sci USA 2013;110(18):7123–30.

[26] Hughes TB, Dang NL, Miller GP, Swamidass SJ. Modeling Reactivity to Biological Macromolecules with a Deep Multitask Network. ACS Cent Sci 2016;2(8):529–37.

[27] FDA. FEARS Pharmacovigilance Database. https://fisfdagov/extensions/FPD-QDE-FAERS/FPD-QDE-FAERShtml. 2022.

[28] Stanford EA, Wang Z, Novikov O, Mulas F, Landesman-Bollag E, Monti S, et al. The role of the aryl hydrocarbon receptor in the development of cells with the molecular and functional characteristics of cancer stem-like cells. BMC Biol 2016;14(1).

[29] Visvader JE. Cells of origin in cancer. Nature 2011;469(7330):314–22.

[30] Eom YH, Kim HS, Lee A, Song BJ, Chae BJ. BCL-2 as a Subtype-Specific Prognostic Marker for Breast Cancer. J Breast Cancer 2016;19(3):252–60.

[31] Pru JK, Kaneko-Tarui T, Jurisicova A, Kashiwagi A, Selesniemi K, Tilly JL. Induction of pro-apoptotic gene expression and recruitment of p53 herald ovarian follicle loss caused by polycyclic aromatic hydrocarbons. Reprod Sci 2009;16(4):347–56.

[32] Huang Y, He J, Liang H, Hu Ke, Jiang S, Yang Lu, et al. Aryl Hydrocarbon Receptor Regulates Apoptosis and Inflammation in a Murine Model of Experimental Autoimmune Uveitis. Front Immunol 2018;9.

[33] Mitsui Y, Chang I, Kato T, Hashimoto Y, Yamamura S, Fukuhara S, et al. Functional role and tobacco smoking effects on methylation of CYP1A1 gene in prostate cancer. Oncotarget 2016;7(31):49107–21.

[34] Li Q, Cheng L, Shen K, Jin H, Li H, Cheng Y, et al. Efficacy and Safety of Bcl-2 Inhibitor Venetoclax in Hematological Malignancy: A Systematic Review and Meta-Analysis of Clinical Trials. Front Pharmacol 2019;10:697.

[35] Maayah ZH, Ghebeh H, Alhaider AA, El-Kadi AOS, Soshilov AA, Denison MS, et al. Metformin inhibits 7,12-dimethylbenz[a]anthracene-induced breast carcinogenesis and adduct formation in human breast cells by inhibiting the cytochrome P4501A1/aryl hydrocarbon receptor signaling pathway. Toxicol Appl Pharmacol 2015;284(2):217–26.

[36] Oakes Samantha R, Gallego-Ortega David, Ormandy Christopher J. The mammary cellular hierarchy and breast cancer. Cellular and Molecular Life Sciences 2014;71:4301–24. doi: https://doi.org/10.1007/s00018-014-1674-4.

[37] Therachiyil Lubna, Roopesh Krishnankutty, Ahmad Fareed, Mateo Jericha M, Uddin Shahab, Korashy Hesham M. Aryl Hydrocarbon Receptor Promotes Cell Growth, Stemness Like Characteristics, and Metastasis in Human Ovarian Cancer via Activation of PI3K/Akt, β-Catenin, and Epithelial to Mesenchymal Transition Pathways. International Journal of Molecular Sciences 2022;23(12):6395. doi: https://doi.org/10.3390/ijms23126395.